

Demonstrating Device-Free Localization based on Radio Tomographic Imaging through Simulations and Experimentation

Pranay Sood

Supervisor: Prof. Ross D. Murch

Department of Electronic and Computer Engineering

August 7, 2020

Agenda



- I. Introduction
- II. The Inverse Scattering Problem
- III. Review of Alternative Approaches
- IV. Radio Tomographic Imaging
- V. Experimental Setup and Results
- VI. Conclusion

Introduction

Section I.



Problem

- Location Based Services (LBSs)
 - Make decisions of plan activities
 - Smart transportsations, households etc.
- Global Positioning System (GPS)
 - Poor accuracy in indoor environments
 - Signal degradation
 - Infeasible in security monitoring, intrusion detection, emergency rescue etc.



Fig. 1.1. Location Based Services¹



Fig. 1.2. Global Positioning System²

¹ "Revenue from location-based services to grow by 25 percent this year in South Korea: Study." News Desk. <https://www.geospatialworld.net/news/revenue-location-based-services-grow-25-percent-year-south-korea-study/> (accessed July 14, 2020)

² "Global Positioning System (GPS) – Architecture, Applications, Advantages." Electricalfundablog. <https://electricalfundablog.com/global-positioning-system-gps/> (accessed July 14, 2020)



Solution

- Device-Free Localization (DFL)
 - Emerging technology
 - Implementation of Wireless Sensor Networks (WSNs)
 - Detect and locate physical objects by measuring changes in received signal strength indicator (RSSI)

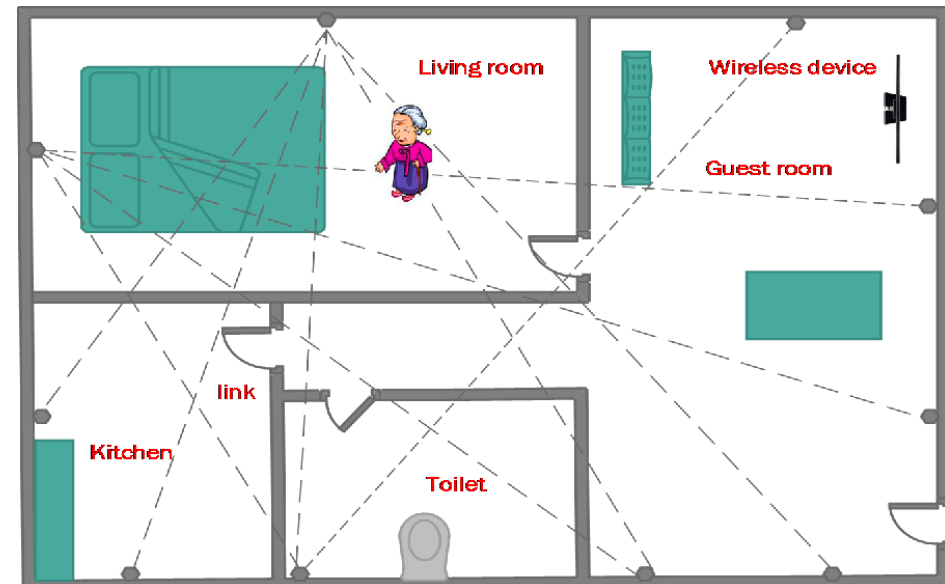


Fig. 1.3. Device-Free Localization³

³ "Nonlinear Optimization-Based Device-Free Localization with Outlier Link Rejection." Semantic Scholar. <https://www.semanticscholar.org/paper/Nonlinear-Optimization-Based-Device-Free-with-Link-Xiao-Song/20cd5e01fe6974de134027cacaf11020646e54bc> (accessed July 14, 2020)



Objectives

- **Background:** Develop understanding of Inverse Scattering Problem and different types of approximation implemented in reconstructing the object with ranges in their size and refractive index
- **Numerical Verification:** Demonstrate DFL using RTI by using exact electromagnetic simulations. We use cylinders with arbitrary size and permittivities and through RTI reconstruction methodology, we can localize the position of the cylinder
- **Experimental Verification:** Discuss and provide details of indoor environment experimentation along with performing a wide range of experimental tests and configurations on the hardware



Challenges

- Inverse Problem
 - Underdetermined Problem
 - Non-linear
- Impact on wireless signals due to:
 - Path Loss
 - Shadowing
 - Multipath Fading
- Limitation in Computing resources
 - 20 hardware modules used for measurements
 - 3D perspective not considered



Contributions

- Utilization of **exact electromagnetic simulations**
 - Implement straightforward exact electromagnetic formulation based on summation of an eigenfunction expansion of the electromagnetic field
 - Derive cylinders with wide range of sizes and permittivities
 - Total variation-based regularization
- Perform experimentation
 - Implementation of inexpensive hardware modules with directional antenna
 - Evaluate hardware modules performance
- Examine inverse scattering
 - Born and Rytov Approximations

Publication from the Research



P. Sood, A. Dubey, C. Chi-Yuk, and R. Murch, "Demonstrating Device-Free Localization based on Radio Tomographic Imaging," *IEEE International Symposium of Antennas and Propagation and North American Radio Science Meeting*. IEEE, 2020. Accepted for publication with paper presentation conducted

The Inverse Scattering Problem

Section II.



Background

- Imaging 3D objects into 2D images
- Computerized Tomography (CT) used for deriving 2D diagnostic images
- Theory of Inverse Scattering known as Diffraction Tomography



Fig. 2.1. X-Ray Image ⁴

⁴ "Generation of the Sinogram." Code Project. <https://www.codeproject.com/Articles/1113200/Computed-Tomography-Generation-of-the-Sinogram-Ima> (accessed July 14, 2020)



Problem Formulation

$$E_{Rx}(\mathbf{r}) = E_{Tx}(\mathbf{r}) + \iiint_D G(\mathbf{r} - \mathbf{r}') f(\mathbf{r}') u(\mathbf{r}') dV(\mathbf{r}')$$

total received field
transmitted incident field
Green's function
material parameter
scattered electromagnetic field

Difficult in determining material parameter and total received field as we only know information outside environment

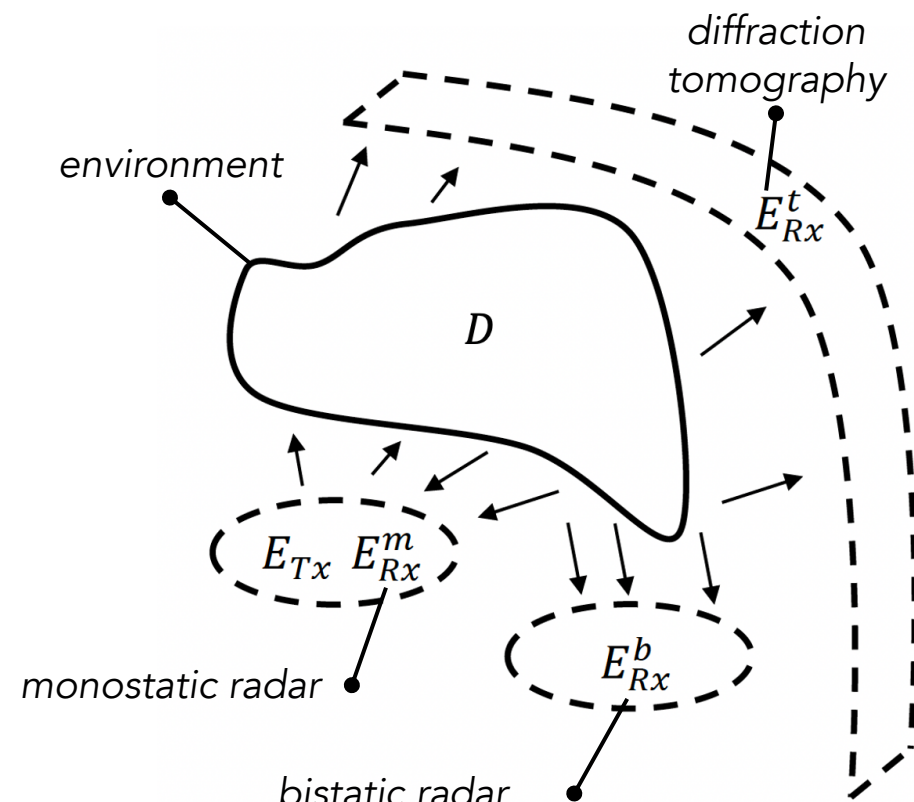


Fig. 2.2. Geometry of Inverse Scattering Problem of environment D [1]

[1] R. Bates, V. Smith, and R. D. Murch, "Manageable multidimensional inverse scattering theory," Physics Reports, vol. 201, no. 4, pp. 185–277, April 1991.



Through-Wall Imaging

Born Approximation

Straightforward relation between received field and scattering cross-section

$$E_{Rx}(\mathbf{r}) = \iiint_D G(\mathbf{r} - \mathbf{r}') f(\mathbf{r}') E_{Tx}(\mathbf{r}') dV(\mathbf{r}')$$

radar cross-section of objects in indoor environment

Rytov Approximation

More precise and incorporates the effect of scattering of all objects

$$E(\mathbf{r}) = E_{Tx}(\mathbf{r}) \exp(j\phi(\mathbf{r}))$$

$$\phi(\mathbf{r}) = \frac{-j}{E_{Tx}(\mathbf{r})} \iiint_D G(\mathbf{r} - \mathbf{r}') f(\mathbf{r}') E_{Tx}(\mathbf{r}') dV(\mathbf{r}')$$



Simulations and Limitations

Simulations

- Radii: 1λ , 2λ , 4λ and 10λ
- Refractive Indexes: 1.001, 1.01, 1.1 and 1.2
 - $\lambda = 0.125 \text{ m}$

Born Approximation

- Quite good at high refractive indexes
 - Fails at cylinders with larger radius

Rytov Approximation

- Excellent reconstructions of cylinders with large radius of 4λ and 10λ
- Fails at high refractive index of 1.1 and 1.2



Straight Ray Approximation

- High frequency signal travelling in direct path from transmitter to receiver
- Basis of RSSI in detecting changes in the environment



Simulation Results

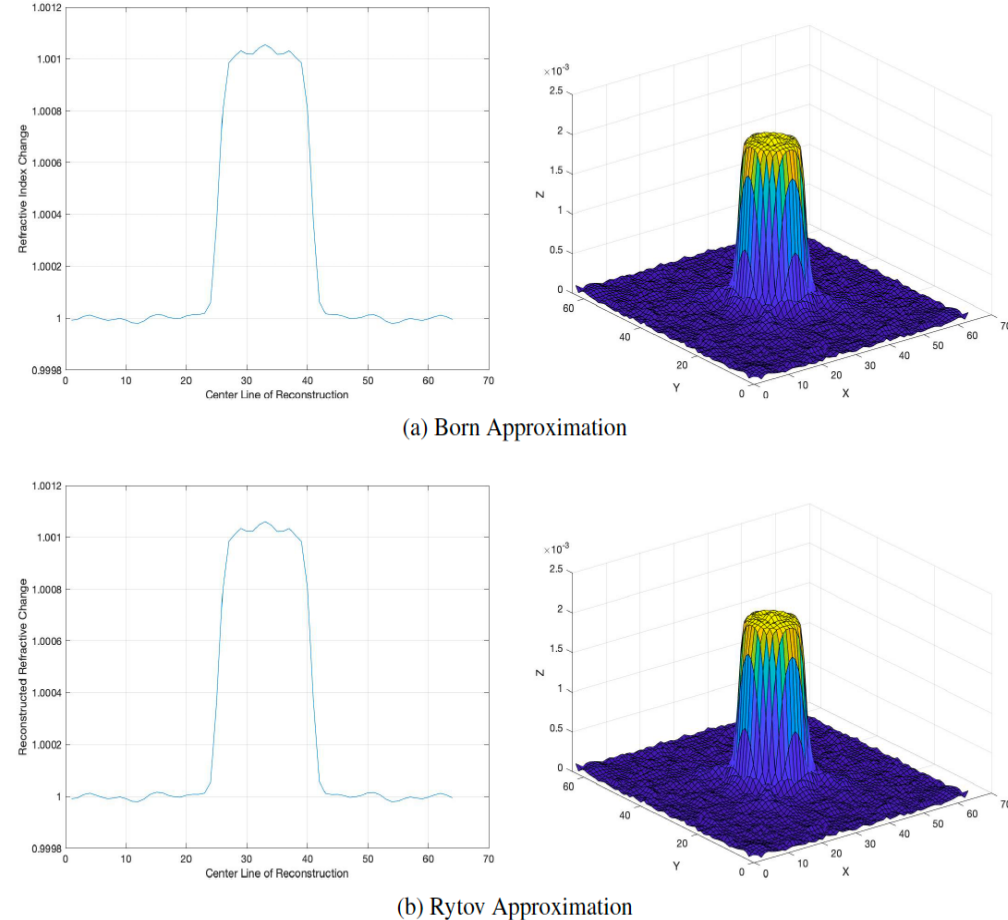


Fig. 2.3. Reconstructions of 4λ with refractive index of 1.001

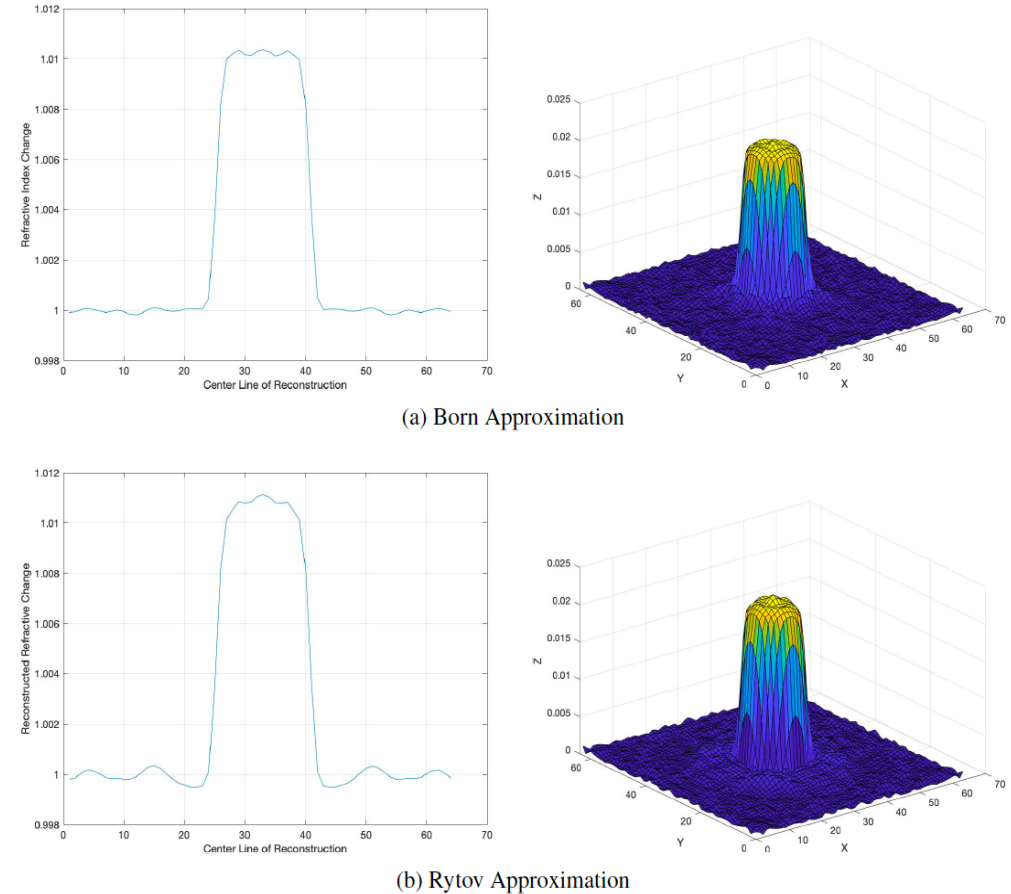


Fig. 2.4. Reconstructions of 4λ with refractive index of 1.01



Simulation Results

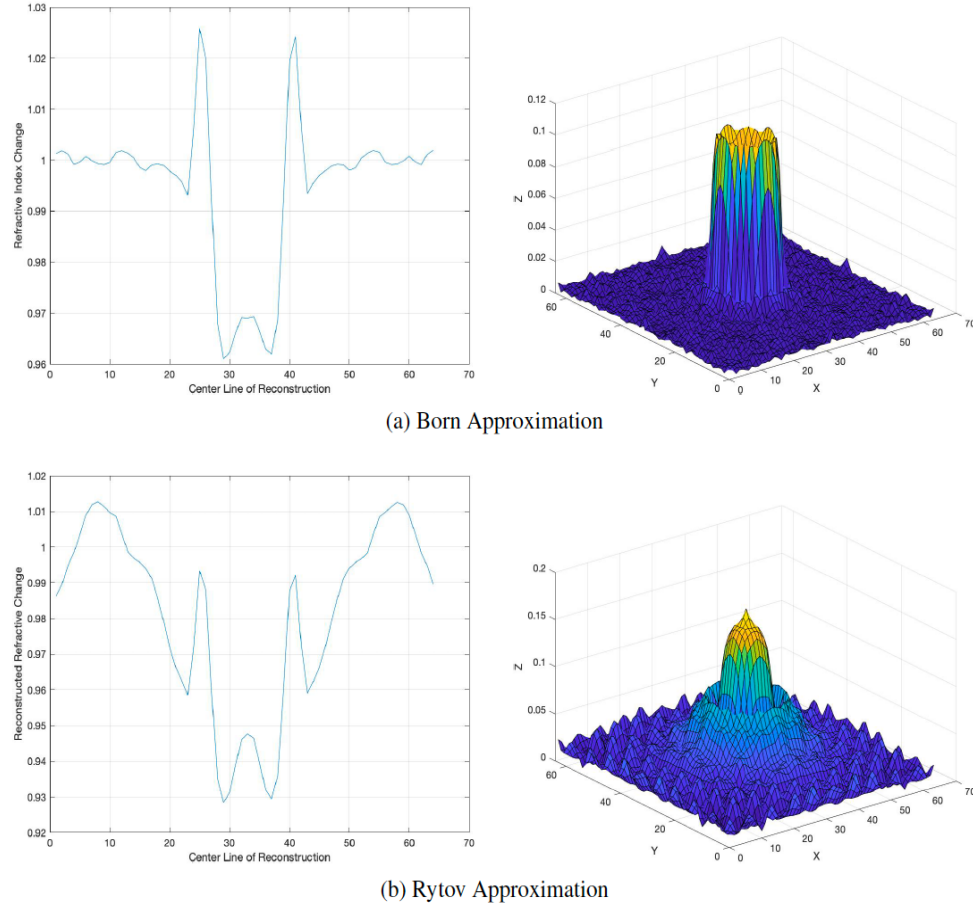


Fig. 2.5. Reconstructions of 4λ with refractive index of 1.1

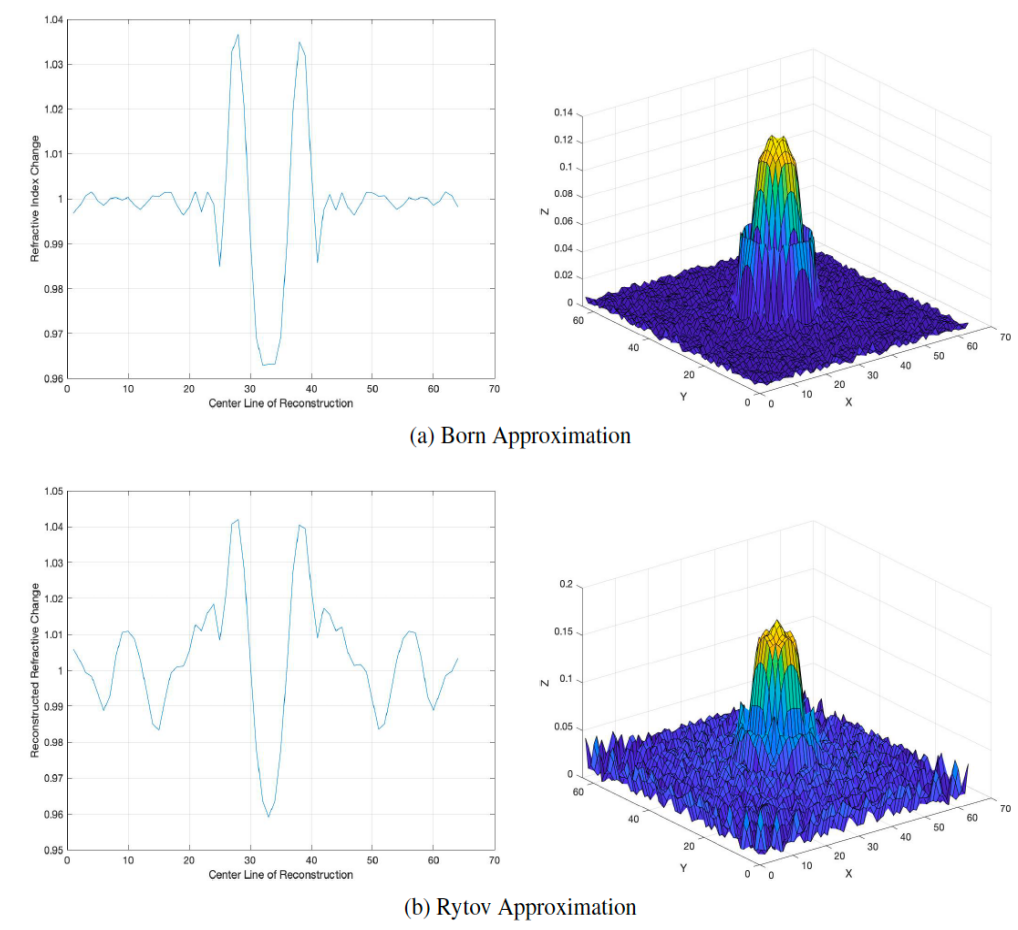


Fig. 2.6. Reconstructions of 4λ with refractive index of 1.2

Review of Alternative Approaches

Section III.

Visual Sensor Networks



- Low power camera nodes to track people
- Large amount of memory data
 - Limitation in network resources
- Deterioration in Image quality
 - Unsuitable in dark regions and environment

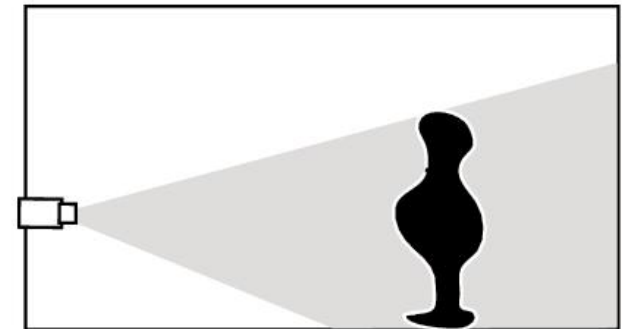
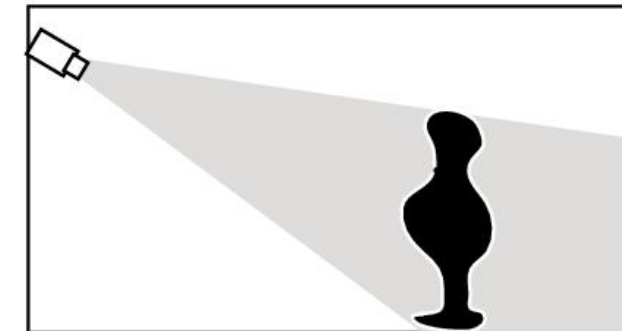


Fig. 3.1. Visual Sensor Network via Two Cameras [2]

[2] S. Soro and W. Heinzelman, "A survey of visual sensor networks," *Advances in Multimedia*, vol. 2009, 06 2009.

Autonomous Robot and RadioBOT



- Autonomous Robots implemented to transmit and receive signal in order to detect RSSI
- Challenges in establishing the hardware and software setup
- Increase in cost
- Not applicable and practical in relation to the WSNs



Fig. 3.3. Autonomous Robot [3]



Fig. 3.4. RadioBOT [4]

[3] S. Depatla, C. R. Karanam, and Y. Mostofi, "Robotic Through-Wall Imaging: Radio-Frequency Imaging Possibilities with Unmanned Vehicles," IEEE Antennas and Propagation Magazine, vol. 59, pp. 47–60, Oct 2017.

[4] B. M. Beck, J. H. Kim, R. J. Baxley, and B. T. Walkenhorst, "RadioBOT: A spatial cognitive radio testbed," in 2013 IEEE Aerospace Conference, pp. 1–9, March 2013.

Fingerprint-based Localization



- RSSI is recorded from a **wide range of access points** and the information is then **stored in a database** along with the coordinates of the object
- RSSI of the **unknown location** is compared to **stored information** in the fingerprint and closest comparison of the match is returned to provide the localization of the object
- Inaccurate results if there is change in the environment
- Database must be updated continuously

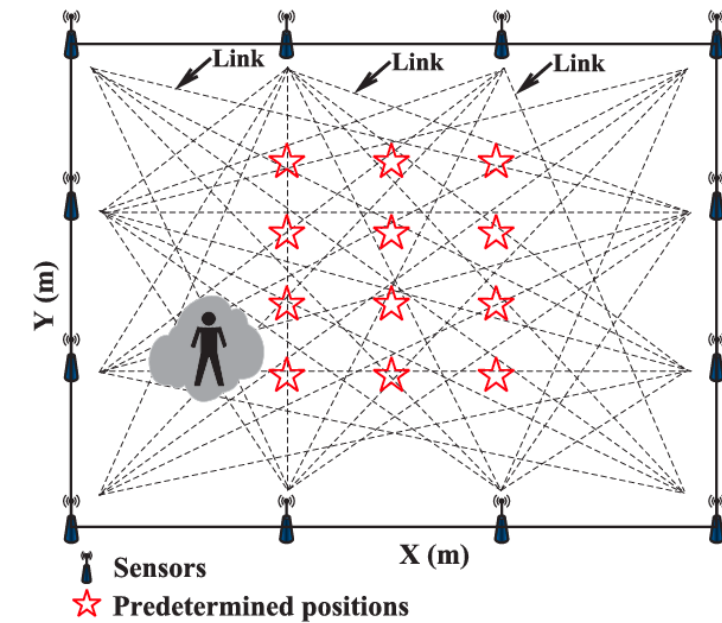


Fig.3.5. Experimentation of Fingerprint-based Localization [5]

[5] Q. Lei, H. Zhang, H. Sun, and L. Tang, "Fingerprint-Based Device-free Localization in Changing Environments Using Enhanced Channel Selection and Logistic Regression," IEEE Access, vol. 6, pp. 2569–2577, 2018.

Radio Tomographic Imaging

Section IV.

Radio Tomographic Imaging (RTI)



- Wi-Fi signals pass through the object in order to obtain the **attenuation** based on the **size and permittivity** of that object
- Reconstruct or image objects using the **line-of-sight (LOS)** shadowing losses measured at sensors in the WSNs
- WSNs in a monitoring area establish wireless links between each sensor to obtain RSSI

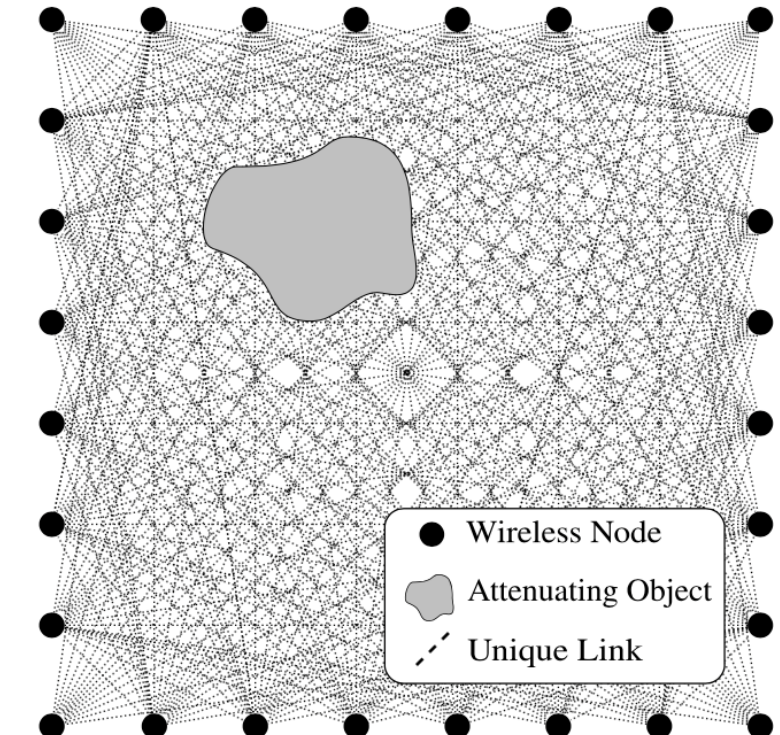


Fig. 4.1. Radio Tomographic Imaging (RTI) Network [6]

[6] J. Wilson and N. Patwari, "Radio Tomographic Imaging with Wireless Networks," IEEE Transactions on Mobile Computing, vol. 9, pp. 621–632, May 2010.



Linear Formulation

$$\text{RSSI} \quad y_i(t) = P_i + S_i(t) + F_i(t) + L_i + v_i(t)$$

- P_i : Transmitted power in decibel-milliwatts (dBm).
- $S_i(t)$: Shadowing loss in dBm that is caused by the presence of an object in the environment thus resulting in signal attenuation.
- $F_i(t)$: Fading loss in dBm due to destructive and constructive interference of Wi-Fi signals in the environment.
- L_i : Static losses in dBm due to distance between Wi-Fi nodes, issues in device hardware and other factors.
- $v_i(t)$: Noise measurement in the environment.

Shadowing Loss

$$\Delta y_i(t) = \sum_{j=1}^N w_{ij} \Delta x_j(t) + n_i$$

attenuation
weighting of pixel j for established node link i
noise



Linear Formulation

RSSI Expression $\Delta\mathbf{y} = \mathbf{W}\Delta\mathbf{x} + \mathbf{n}$

$$\Delta\mathbf{y} = [\Delta y_1, \Delta y_2, \dots, \Delta y_M]^T$$
$$\Delta\mathbf{x} = [\Delta x_1, \Delta x_2, \dots, \Delta x_N]^T$$
$$\mathbf{n} = [n_1, n_2, \dots, n_M]^T$$
$$\mathbf{W} = [w_{ij}]_{M \times N}$$

K • Wi-Fi nodes deployed

M • total number of unique two-way wireless links $M = \frac{K^2 - K}{2}$

N • square pixels

$\Delta\mathbf{y}$ • change in RSSI measurement of M links

$\Delta\mathbf{x}$ • shadowing and attenuation caused by the object to be estimated

\mathbf{W} • weight matrix with $M \times N$ dimension with columns representing the pixels and row representing the weight for each pixel for which a particular link passes through

\mathbf{n} • Noise (can be considered negligible)

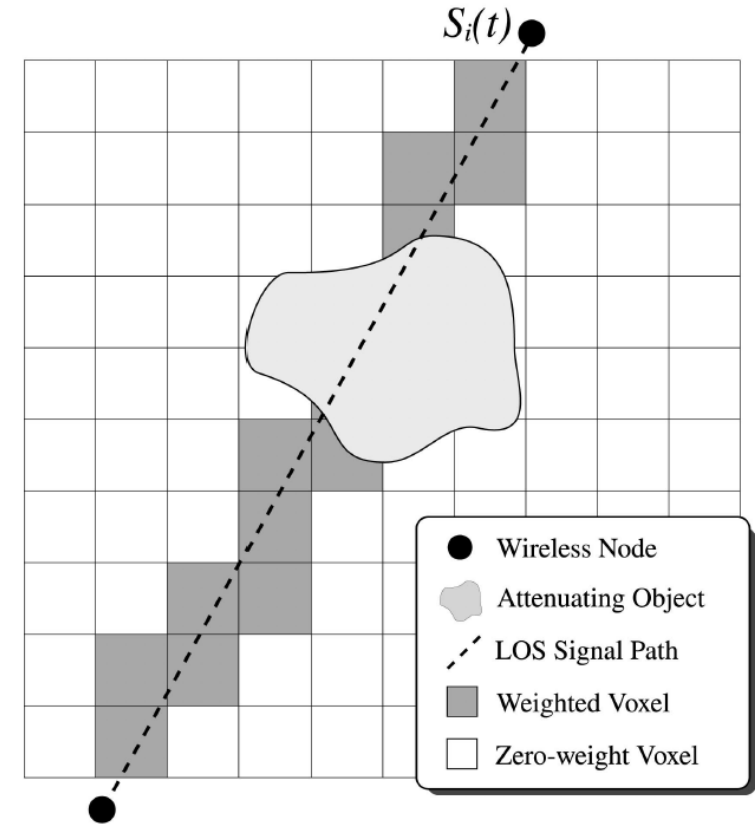


Fig. 4.2. Single link present in an RTI Model [6]

[6] J. Wilson and N. Patwari, "Radio Tomographic Imaging with Wireless Networks," IEEE Transactions on Mobile Computing, vol. 9, pp. 621–632, May 2010.



Weight Model

Normalized Weight

$$\mathbf{w}_{ij} = \frac{1}{\sqrt{d}} \begin{cases} 1 & \text{if } d_1 + d_2 < d + \delta \\ 0 & \text{otherwise} \end{cases}$$

where d is the distance between two nodes, d_1 and d_2 are distances from pixel j and the two nodes respectively for link i . δ is a tunable parameter which is the width of the ellipse.

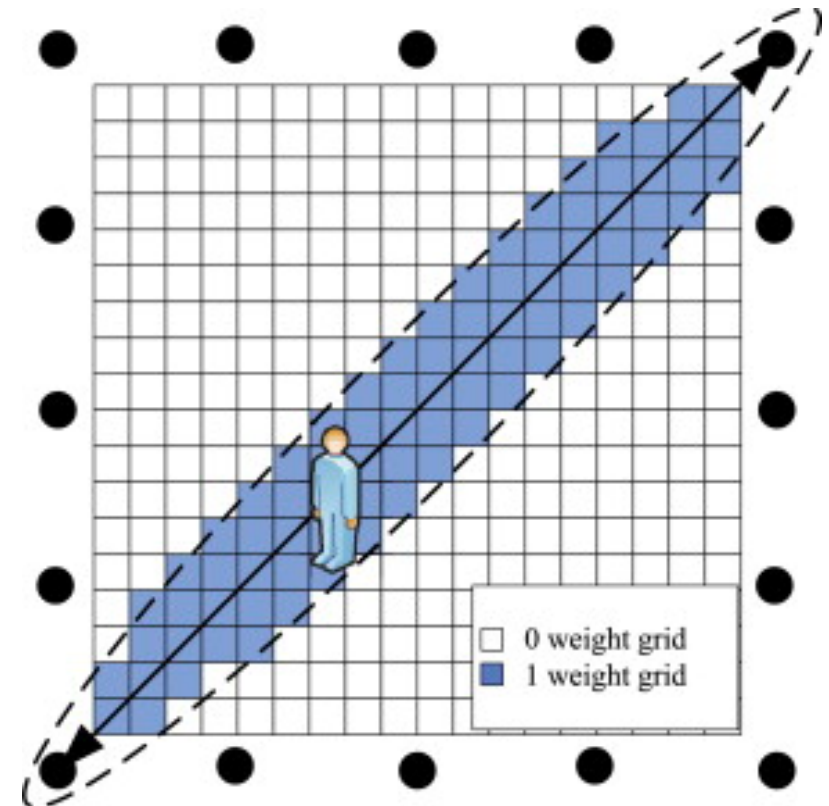


Fig. 4.3. Weighting Model of RTI [7]

[7] Z. Wang, H. Liu, X. Ma, J. An, and S. Xu, "Enhancing indoor radio tomographic imaging based on interference link elimination," Digital Signal Processing, vol. 44, pp. 26 – 36, 2015.



Simulation Setup

- Electromagnetic Simulation
 - $3m$ by $3m$ by $4m$ (*room height*) $\sim 24\lambda$ by 24λ by 32λ ($\approx 18500\lambda^3$)
- Simplify the object of interest in the room by using a **2D approach** and **dielectric cylinder** at any location with a **fixed radius** and **varying permittivity**
- Use **exact eigenfunction expansions** to efficiently and accurately estimate the RSSI
- At 2.4 GHz , Objects such as furniture and humans in the room are taken to have permittivity ranging from 1.5 to 30 and cylinder radius $0.3m$

[8] D. S. Jones, Methods in Electromagnetic Wave Propagation. Oxford: Oxford University Press, 1979.

Simulation Setup



$K = 20$ Wi-Fi Nodes

$M = 190$ unique two-way wireless links
Cylinder centered at (2,2)

Permittivities	Object Representation
1.5	Object such as Styrofoam
3	Object such as Wooden Furniture
30	Humans or objects with high water content

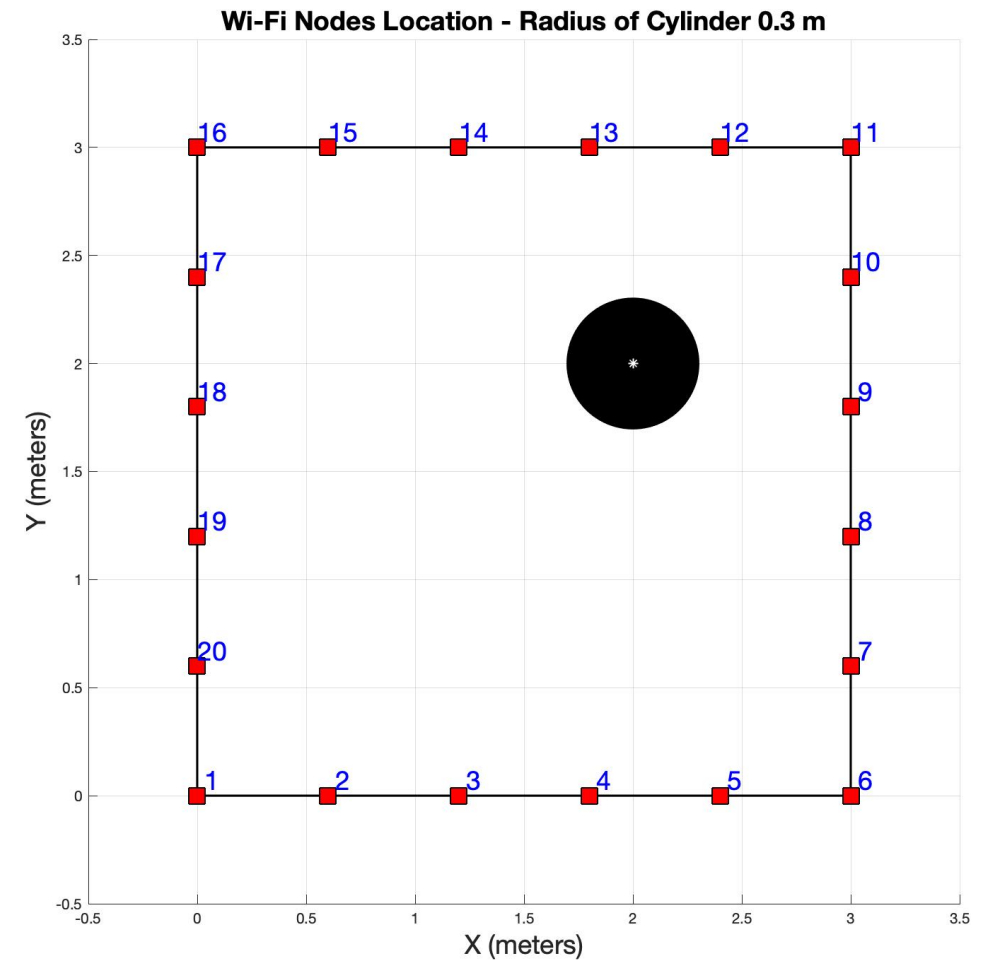


Fig. 4.4. Setup of the Simulation

III-Posed Inverse Problem – Least-Squared-Error



Least-squared approach

$$\mathbf{x}_{LS} = \arg \min_{\mathbf{x}} \|\mathbf{Wx} - \mathbf{y}\|_2^2$$

$$\mathbf{x}_{LS} = (\mathbf{W}^T \mathbf{W})^{-1} \mathbf{W}^T \mathbf{y}$$

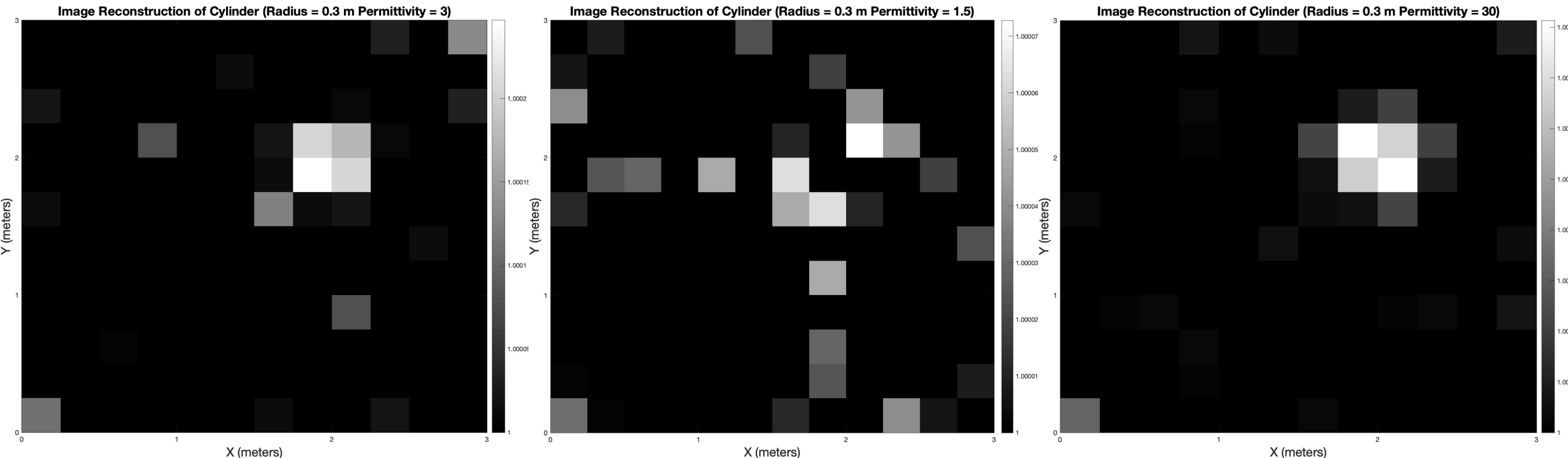


Fig. 4.5. Reconstruction of cylinders with radius 0.3 m with wide range of permittivities at grid size of 0.25

III-Posed Inverse Problem – Total Variation Based Regularization



- Issue: Detect change in the environment with higher resolution
 - $M = 190$ – Maximum resolution $\approx 0.21m$ by $0.21m$ ($N \approx 190$)
 - Pixel size: $0.1m$ by $0.1m$ ($N = 900$)
 - Underdetermined Problem – ($M = 190, N = 900, N \gg M$)
- Number of unknowns is larger than number of measurements, regularization performed with only **21%** measurements
- Solution – Total variation-based regularization:

$$\mathbf{x}_{TVAL} = \arg \min_{\mathbf{x}} \|\mathbf{y} - \mathbf{Wx}\|_2^2 + \alpha \|\mathbf{Dx}\|_1$$

α —————• regularization parameter

\mathbf{D} —————• difference between successive elements of $\Delta \mathbf{x}$



Simulation

$$\mathbf{x}_{TVAL} = \arg \min_{\mathbf{x}} \|\mathbf{y} - \mathbf{Wx}\|_2^2 + \alpha \|\mathbf{Dx}\|_1$$

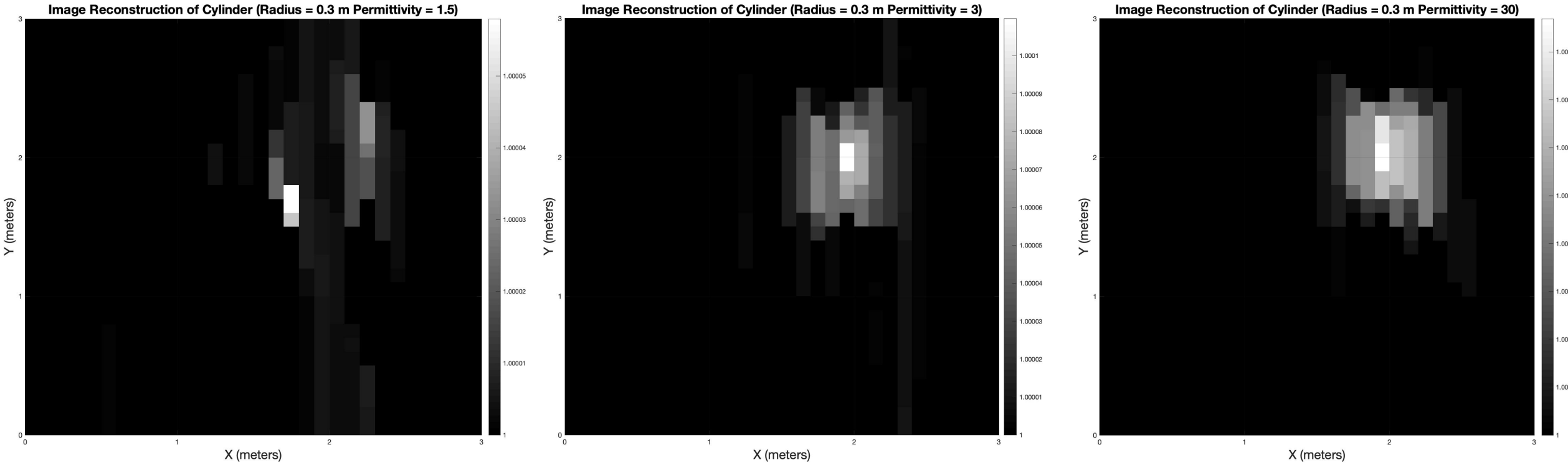


Fig. 4.6. Reconstruction of cylinders with radius 0.3 m with wide range of permittivities at grid size of 0.01

Experimental Setup and Results

Section V.

Multiple Wi-Fi Node Measurement System



- Design Aim
 - Wi-Fi module as an **Access Point (AP)**, thus making it a
 - Suitable portal for devices to connect to a local area network
 - AP beacon signal to determine RSSI levels
 - Wi-Fi module also configured as a **Station (STA)**
 - Can act as a wireless client and connect to other APs or Routers
 - Possible to scan Wi-Fi channels to obtain RSSI levels from other nodes
 - Data from each Wi-Fi node sent to server via Wi-Fi Router and stored as file
 - N nodes will result in $N^2 - N$ unique RSSI measurements for every scan cycle



Hardware Details

- SparkFun ESP32 Thing Board
 - Power and versatility hence suitable for IoT
 - Inexpensive and not complex to configure and program
- Directional Antenna
 - FR4 Epoxy Board
 - Inexpensive
 - High fabrication tolerances

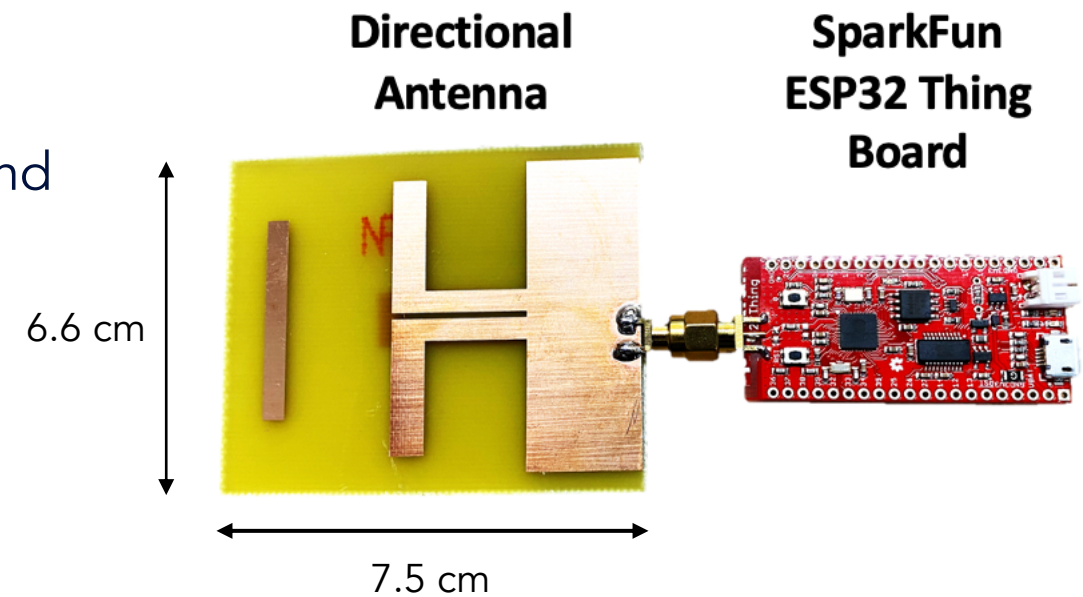


Fig. 5.1. Eletromechanical fixture between SparkFun ESP32 Thing Board and Directional Antenna



Hardware Details – Directional Antenna

- Gain at 2.4 GHz is 6.6 dBi
- Minimum ground reflections
 - Less impact of multipath fading
- Minimal gain at backside of directive antenna
 - Minimizing reflections of wall
- Reduction in scattering due to high gain thus linearize RTI model performs better

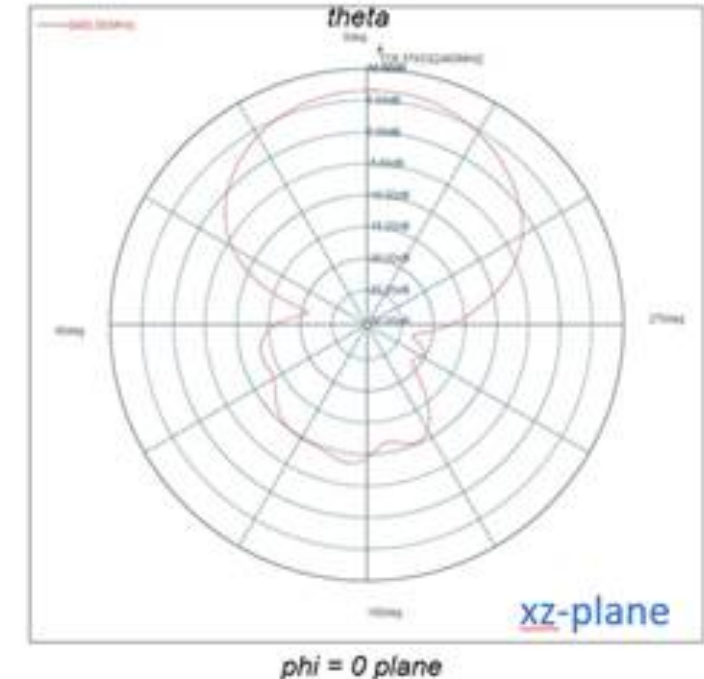


Fig. 5.2. Radiation pattern of directive antenna position at $\phi = 0$ place



System Setup

- ESP32 Board and Directional Antenna
 - C++ code uploaded and compiled via Arduino IDE
 - Distinct board numbers
 - Running in AP and STA mode to be connected to Wi-Fi router and act as own AP
 - Scan area for APs with SSID that contains keyword "Measure"
 - SSIDs and RSSI of individual unique SSID stored in array and sent Server through the AP
 - Every 10 seconds, all boards have transmitted and received RSSI
 - One board acts as a transmitter and other boards act as receivers
 - Theory of Reciprocity



Fig. 5.2. ESP32 Boards with Directional Antenna positioned around a domain

[9] R. D. Murch, "Multiple Wi-Fi Node Measurement System," pp. 1–6, February 2019.



System Setup

- Wi-Fi Router
 - Own SSID name and password
 - Bounded to MAC Address of Server through IP Address
- Remote PC (Server)
 - Server established and programmed in Python language
 - Code executed in Remote PC terminal with data processed and stored in a log file
 - Log file stored in folders to keep track of time when data is being collected while performing experiment
 - MATLAB code used to further process the raw data collected

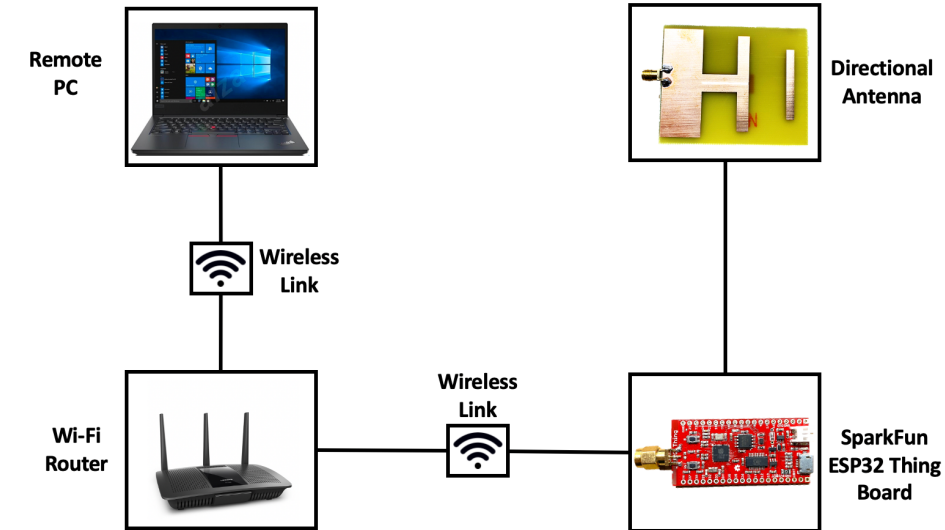


Fig. 5.3. Block Diagram of the Wi-Fi Node Measurement System

[9] R. D. Murch, "Multiple Wi-Fi Node Measurement System," pp. 1–6, February 2019.



Experimental Tasks and Procedures

- Experiment One
 - Two ESP32 Boards placed opposite to each other with changing distance of separation
 - Mean and standard deviation of RSSI levels measured and compared with two-ray ground-reflection model
- Experiment Two
 - Two ESP32 Boards placed 3 m apart with objects of wide range of permittivities introduced
- Experiment Three
 - 20 ESP32 Boards placed around a 3 m by 3 m region to obtain the RSSI measurements of different situations:
 - Empty region with no physical object present
 - Presence of one human
 - Presence of two humans at different locations
 - Presence of box filled with water



Two-Ray Ground-Reflection Model

$$P_r = P_t \left[\frac{\lambda}{4\pi} \right]^2 \left| \frac{\sqrt{G_{los}}}{d_{los}} + R \frac{\sqrt{G_{ref}} \exp(-j\phi)}{d_{ref}} \right|^2$$

where:

$$\sqrt{G_{los}} = \sqrt{G_a G_b}$$

$$\sqrt{G_{ref}} = \sqrt{G_c G_d}$$

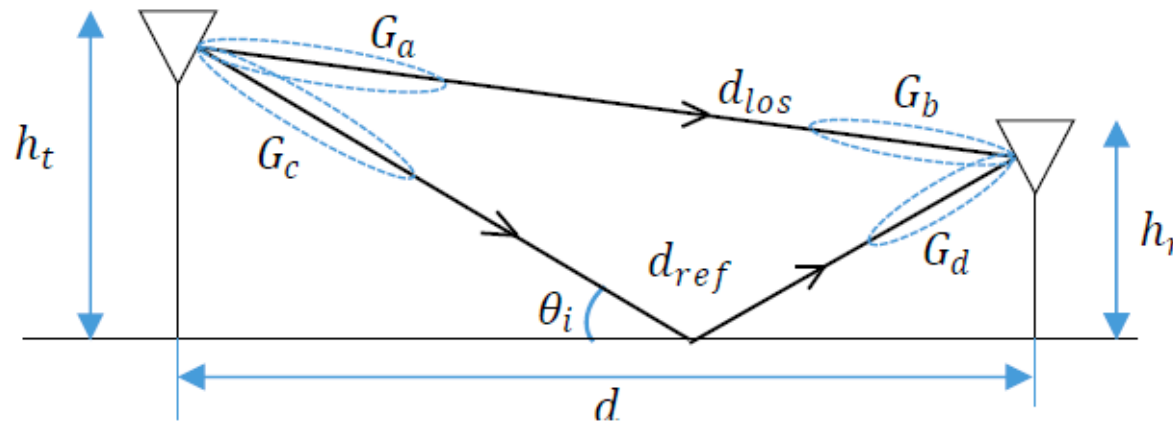


Fig. 5.4. Two-ray ground-reflection model [14]

$$d_{los} = \sqrt{d^2 + (h_t - h_r)^2}$$

$$d_{ref} = \sqrt{d^2 + (h_t + h_r)^2}$$

$$\phi = \frac{2\pi(d_{ref} - d_{los})}{\lambda}$$

Two – ray interference model depending on the phase difference ϕ between LOS and reflected ray

P_t : Transmitted Power

P_r : Received Power

d : Distance between h_t and h_r

λ : Wavelength

h_t : Height of Transmitter

h_r : Height of Receiver

R : Ground Reflection Coefficient

G_{los} : Gain of LOS Ray

G_{ref} : Gain of Reflected Ray

[10] M. Viswanathan, "Two ray ground reflection model." <https://www.gaussianwaves.com/2019/03/two-ray-ground-reflection-model/>, 2019. Accessed: 2020-06-20.

Two-Ray Ground-Reflection Model Simulation



$$P_r = P_t D_t D_r \left[\frac{\lambda}{4\pi} \right]^2 \left| \frac{1}{d_{los}} + R \frac{\exp(-j\phi)}{d_{ref}} \right|^2$$

$$P_t = 19.5 \text{ dBm}$$

$$\lambda = 0.125 \text{ m}$$

$$h_t = 1.2 \text{ m}$$

$$h_r = 1.2 \text{ m}$$

$$R = 0, -\frac{1}{4}, -\frac{1}{2}, -1$$

$$G_{los} = G_{ref} = 1 \sim \text{negligible}$$

D_t : Directivity of transmitting antenna = 6.6 dB

D_r : Directivity of receiving antenna = 6.6 dB

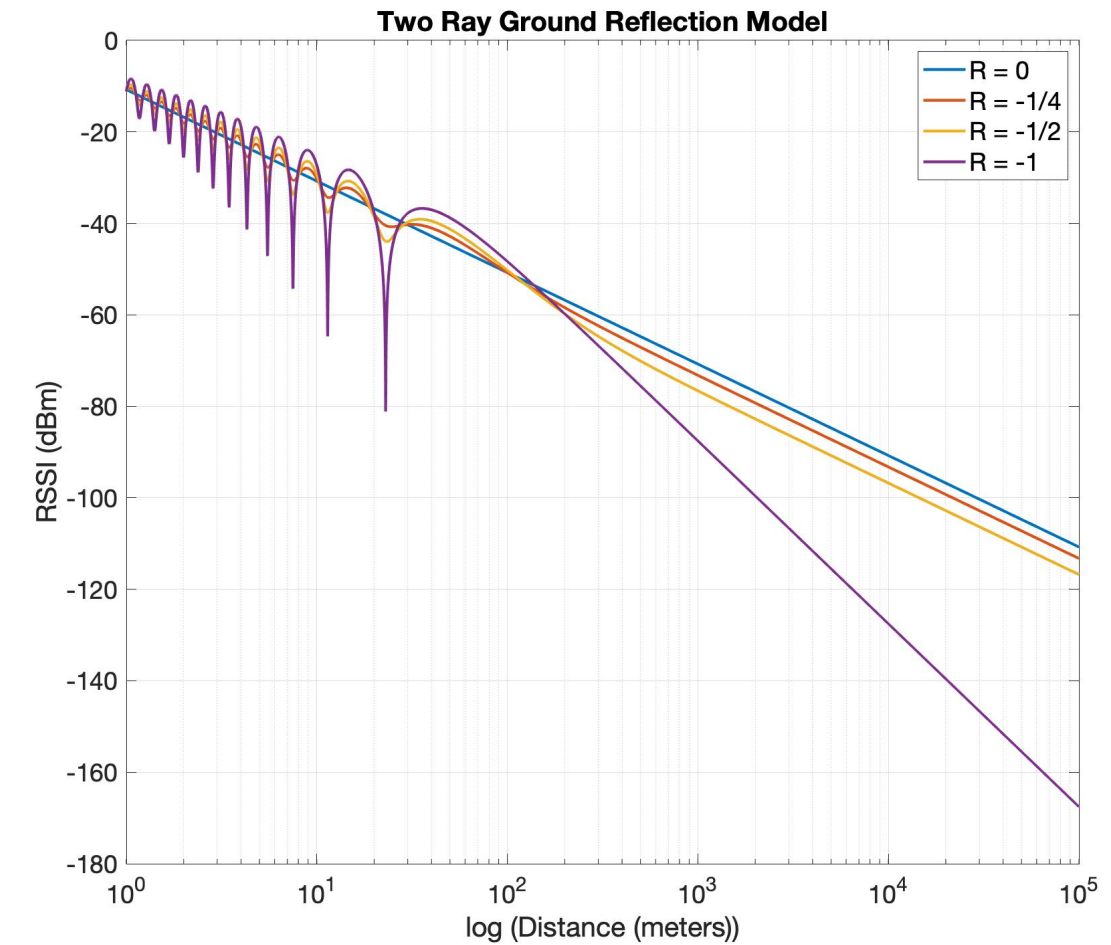


Fig. 5.5. Simulation of two-ray ground-reflection model with wide range of R

Experiment One – Results



- Mean RSSI

Decrease in RSSI as distance of separation increases



Fig. 5.6. Two ESP32 Boards placed opposite of each other

- Standard Deviation

Less than 1 dBm
Directional antenna reduced impact of multipath fading

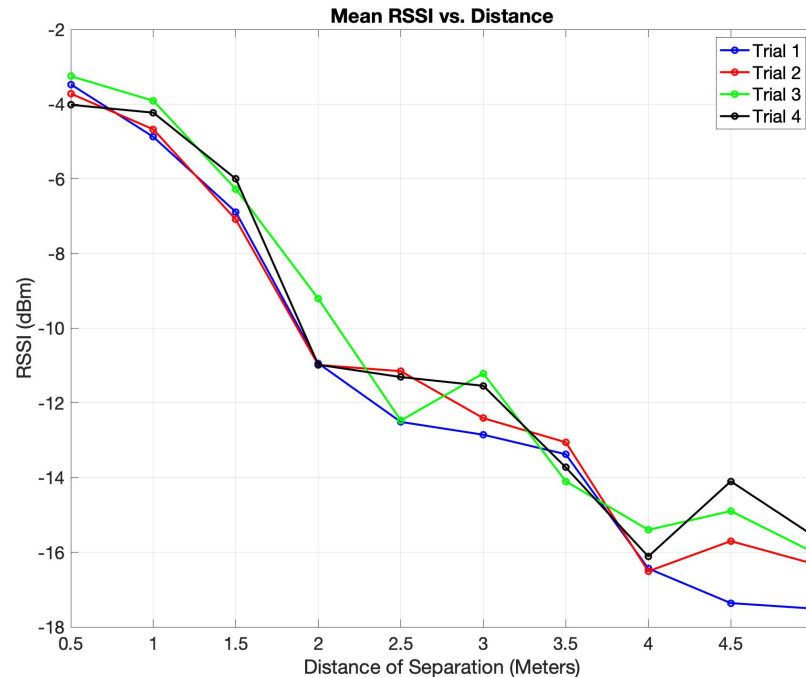


Fig. 5.7. Mean RSSI

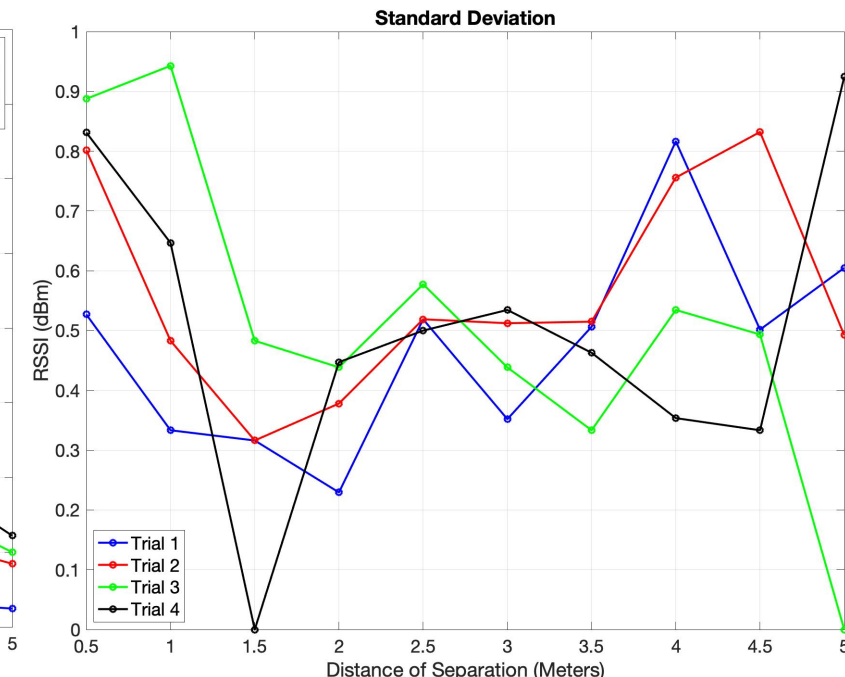


Fig. 5.8. Standard Deviation of RSSI

Experiment One – Comparison Results



- Small difference between experimental results and two-ray ground-reflection model
- Earlier using ESP32 Board in-built Omnidirectional Antenna
 - Impact of multipath fading (ground reflections) is significant thus being problematic
- Directional Antenna reduces the impact of multipath fading

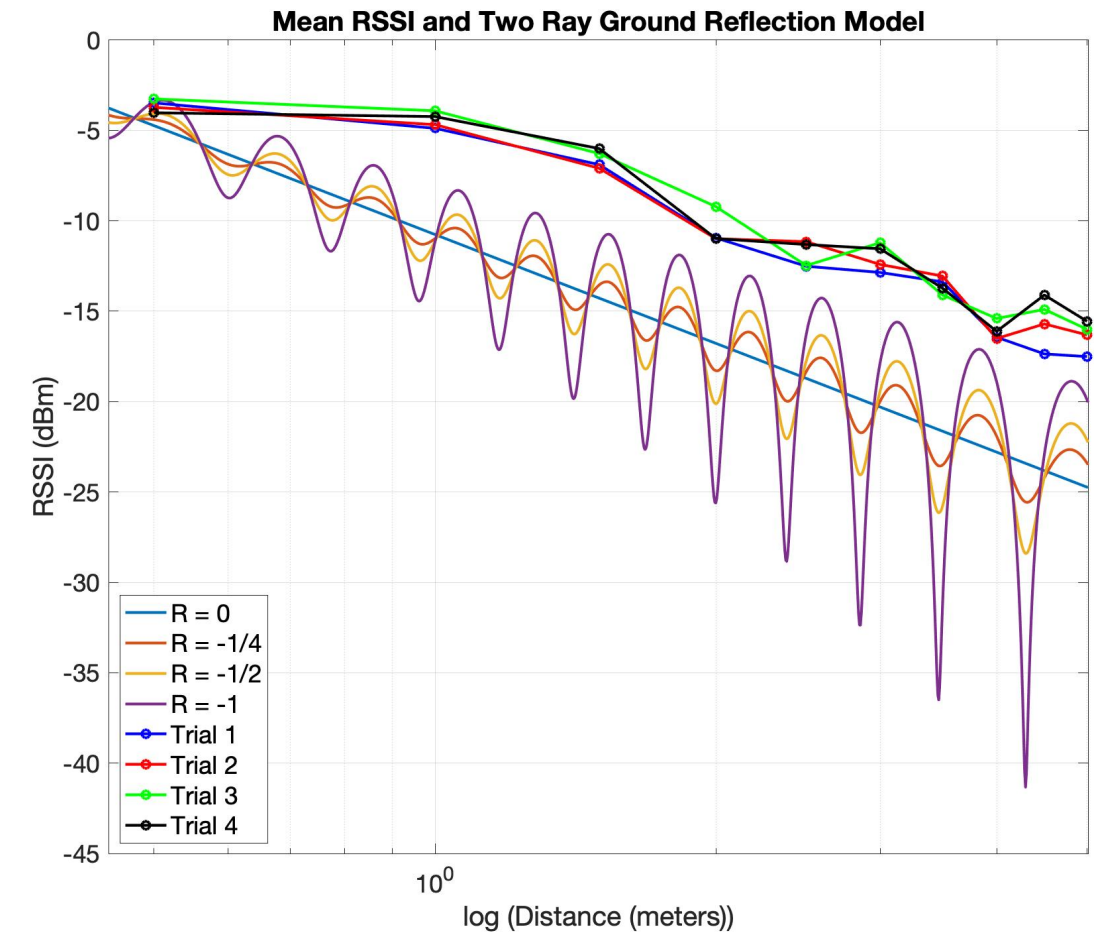


Fig. 5.9. Comparison between two-ray ground-reflection model and mean RSSI results



Experiment Two Results

Wooden Table

- Permittivity ranging from 2 to 6

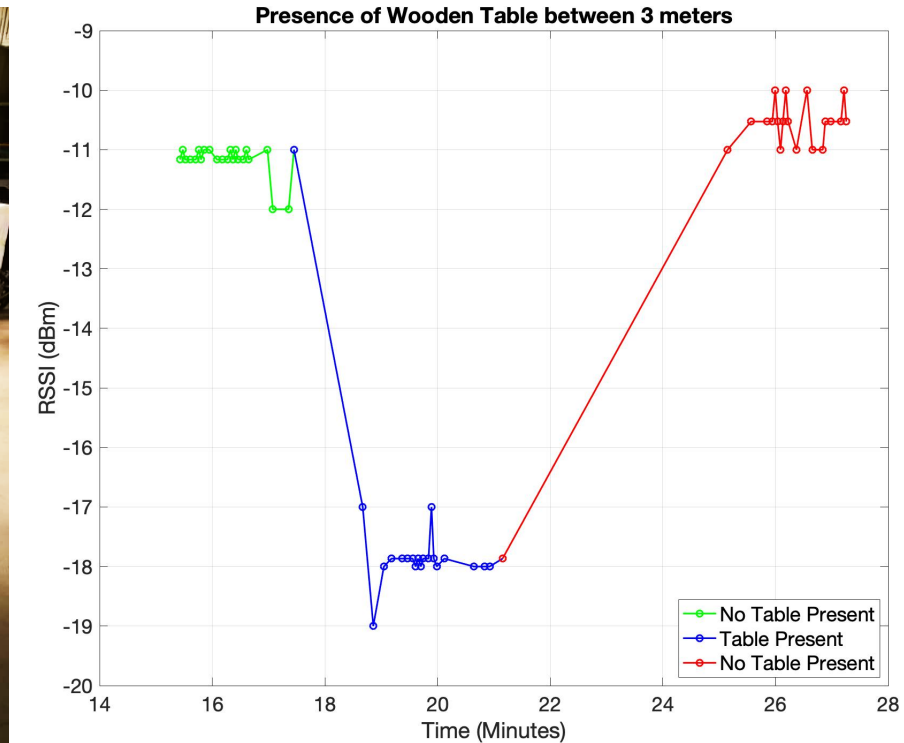


Fig. 5.10. Result of Wooden Table present between two ESP32 Boards



Experiment Two Results

Humans

- High water content
- Permittivity ranging from 20 to 60

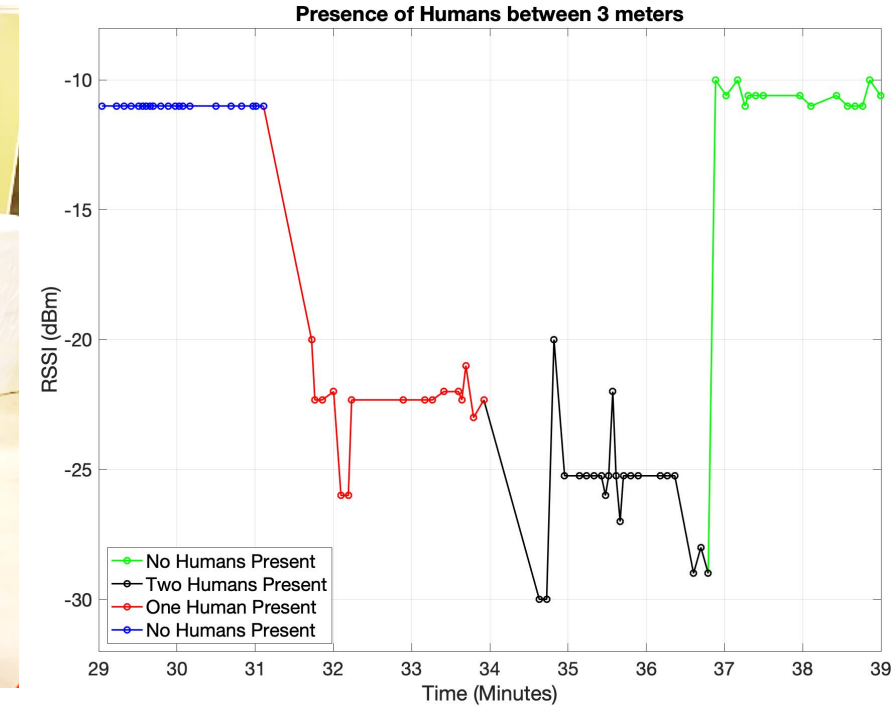


Fig. 5.11. Result of One Human and Two Humans present between two ESP32 Boards

Experiment Three Results

Empty Region

- 3m by 3m domain of interest
 - 20 ESP32 Boards utilized



Fig. 5.12. 20 ESP32 Boards placed around a surrounding of 3m by 3m.

RSSI Readings

- 10 minutes data collected
 - Anomalies present
 - Mode matrix obtained

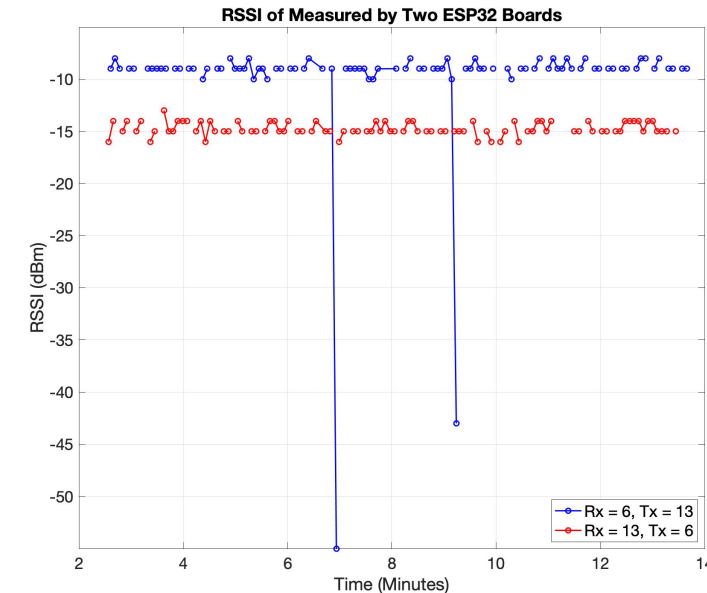


Fig. 5.13. RSSI readings between two ESP32 Boards numbered 6 and 13.



Experiment Three Results

Individual positioned at **(1.2, 1.2)**

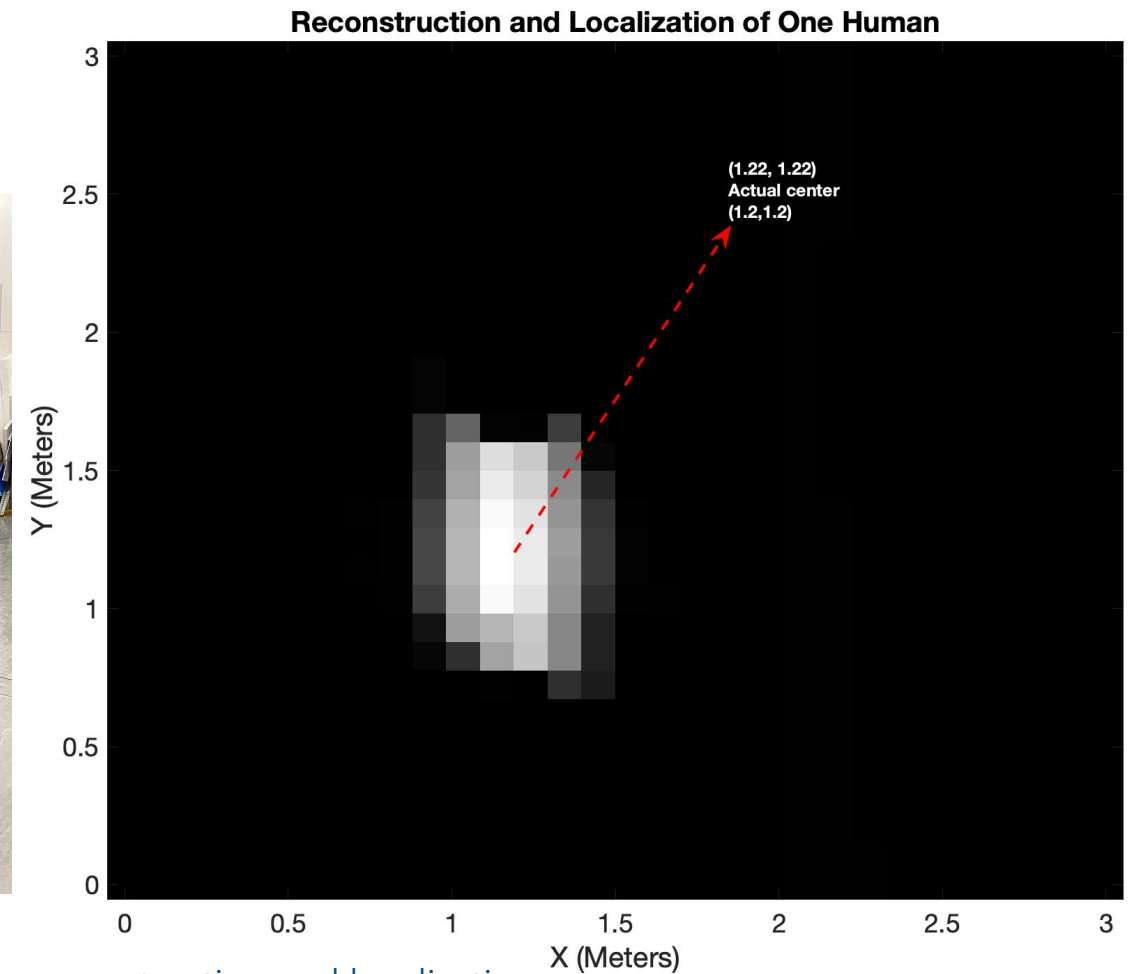


Fig. 5.14. Result of **One Human** reconstruction and localization



Experiment Three Results

Human 1 positioned at **(1.2, 1.2)**

Human 2 positioned at **(2.4, 1.8)**

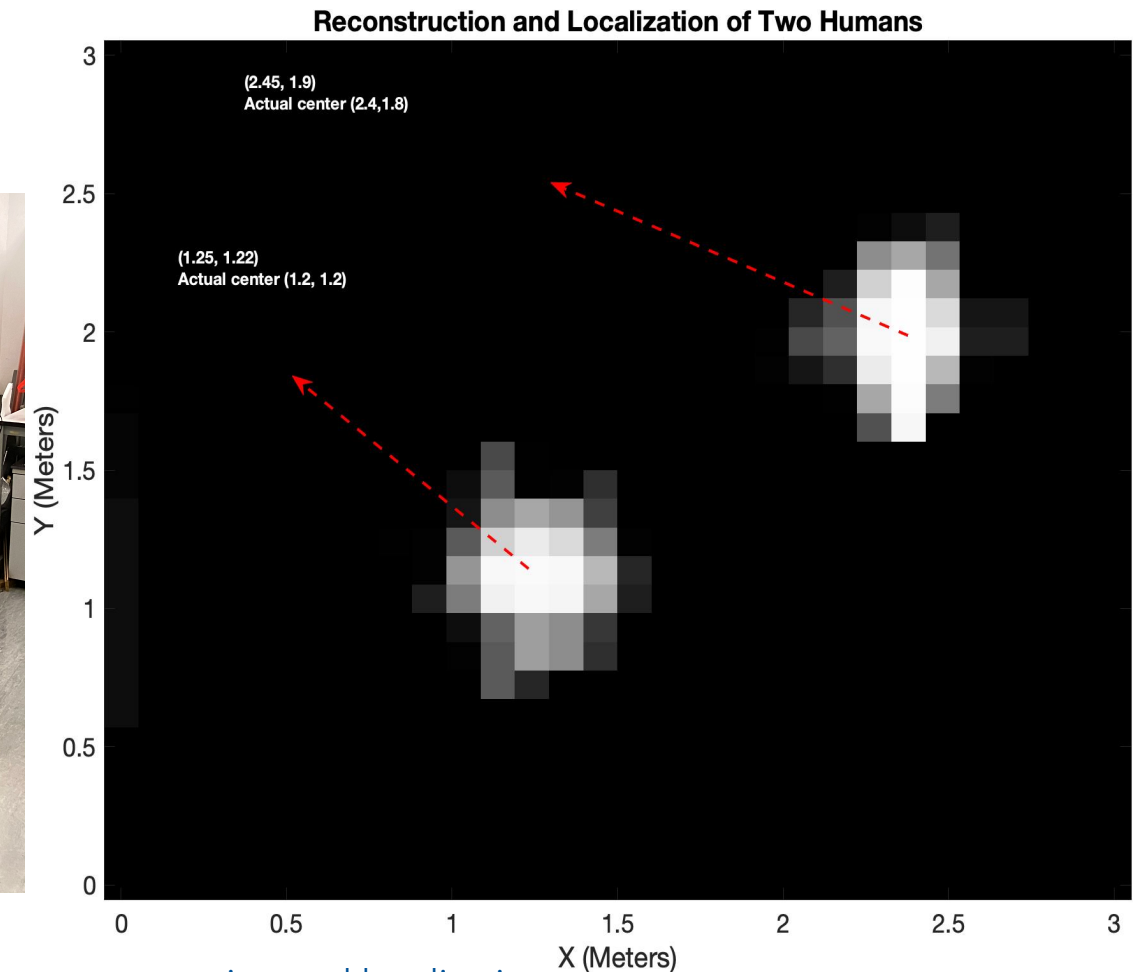
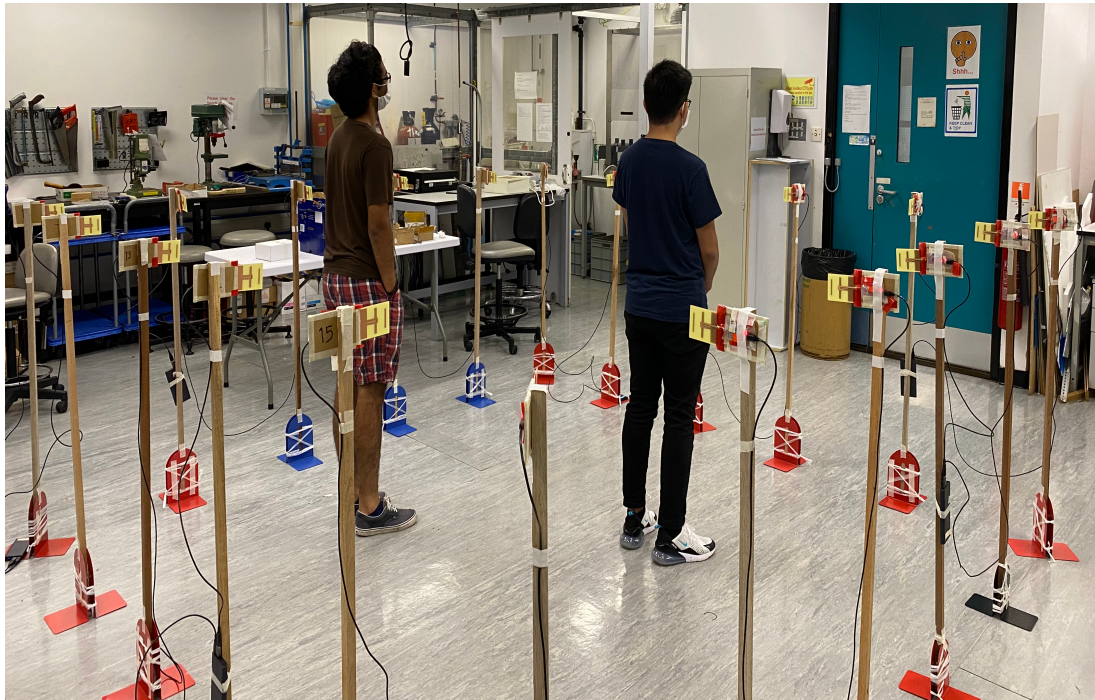


Fig. 5.15. Result of **Two Humans** reconstruction and localization

Experiment Three Results

Box filled with Water
positioned at (1.5, 1.5)

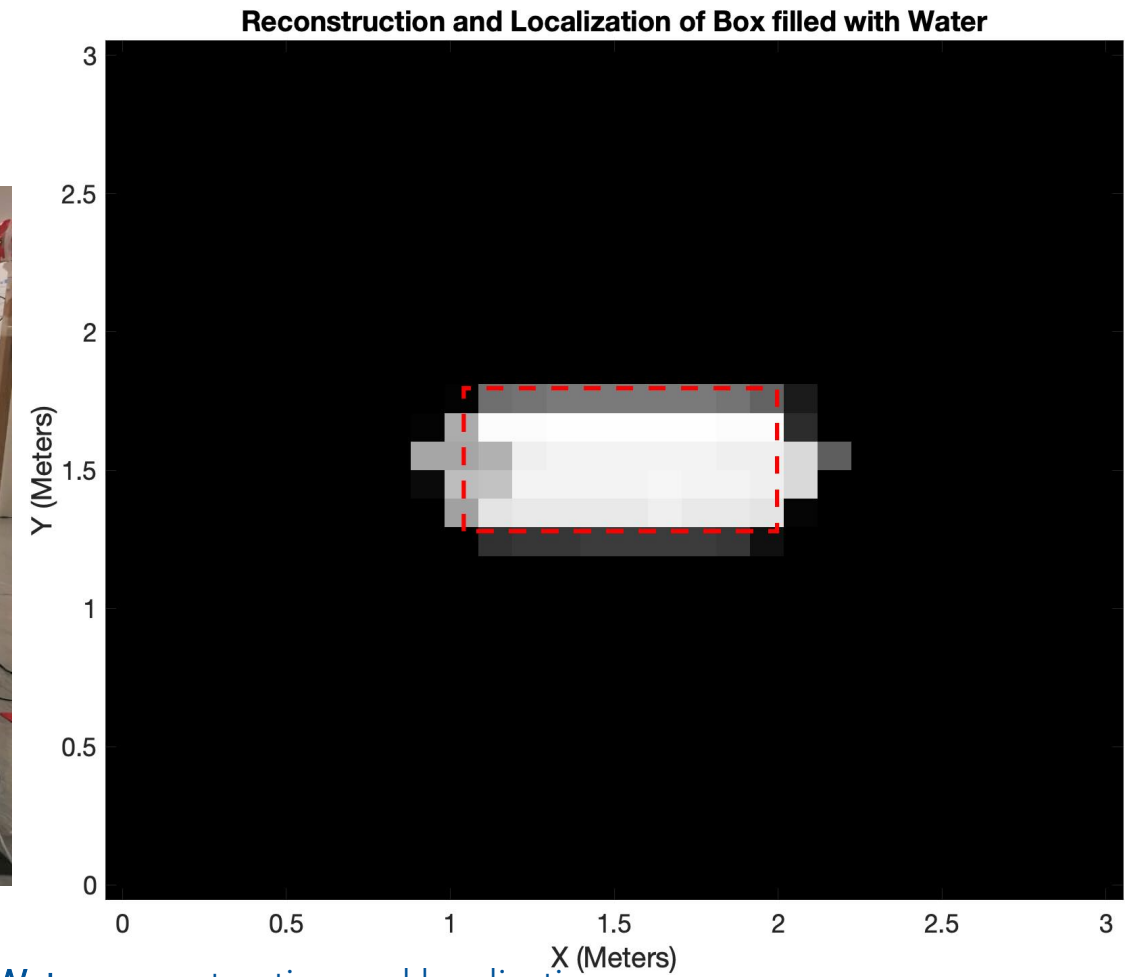
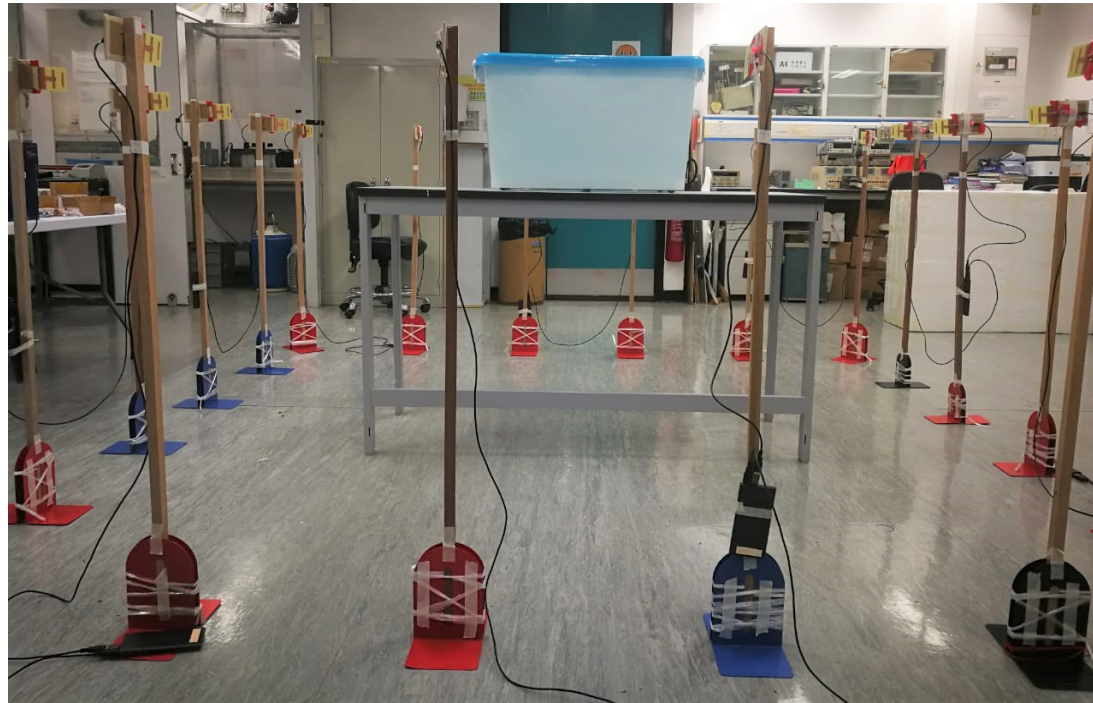


Fig. 5.16. Result of Box filled with Water reconstruction and localization

Conclusion

Section VI.

Conclusion & Future Work



Contributions

- Perform electromagnetic simulations to generate dielectric cylinders in order to reconstruct and localize the position of the cylinder at high resolution via total variation-based regularization
- Develop an experimental setup with inexpensive hardware modules to ensure that physical objects present in the region at different coordinates can be reconstructed and localized

Key Takeaways for Future Study

- Implementation of more Wi-Fi modules for more data collection
- RTI fails at permittivity of less than 3
- Phase measurements not considered in RTI
- Explore more inverse scattering techniques
- Possibility of exploring a model that is a combination of LOS based RTI and Rytov Approximation

References



References

- [1] R. Bates, V. Smith, and R. D. Murch, "Manageable multidimensional inverse scattering theory," *Physics Reports*, vol. 201, no. 4, pp. 185–277, April 1991.
- [2] S. Soro and W. Heinzelman, "A Survey of Visual Sensor Networks," *Advances in Multimedia*, vol. 2009, 06 2009.
- [3] S. Depatla, C. R. Karanam, and Y. Mostofi, "Robotic Through-Wall Imaging: Radio-Frequency Imaging Possibilities with Unmanned Vehicles," *IEEE Antennas and Propagation Magazine*, vol. 59, pp. 47–60, Oct 2017.
- [4] B. M. Beck, J. H. Kim, R. J. Baxley, and B. T. Walkenhorst, "RadioBOT: A spatial cognitive radio testbed," in *2013 IEEE Aerospace Conference*, pp. 1–9, March 2013.
- [5] Q. Lei, H. Zhang, H. Sun, and L. Tang, "Fingerprint-Based Device-free Localization in Changing Environments Using Enhanced Channel Selection and Logistic Regression," *IEEE Access*, vol. 6, pp. 2569–2577, 2018.
- [6] J. Wilson and N. Patwari, "Radio Tomographic Imaging with Wireless Networks," *IEEE Transactions on Mobile Computing*, vol. 9, pp. 621–632, May 2010.
- [7] Z. Wang, H. Liu, X. Ma, J. An, and S. Xu, "Enhancing indoor radio tomographic imaging based on interference link elimination," *Digital Signal Processing*, vol. 44, pp. 26 – 36, 2015.
- [8] D. S. Jones, *Methods in Electromagnetic Wave Propagation*. Oxford: Oxford University Press, 1979.
- [9] R. D. Murch, "Multiple Wi-Fi Node Measurement System," pp. 1–6, February 1991.
- [10] M. Viswanathan, "Two ray ground reflection model." <https://www.gaussianwaves.com/2019/03/two-ray-ground-reflection-model/>, 2019. Accessed: 2020-06-20.

References



- [11] D. Yu, Y. Guo, N. Li, and D. Fang, "Dictionary Refinement for Compressive Sensing Based Device-Free Localization via the Variational EM Algorithm," *IEEE Access*, vol. 4, pp. 9743–9757, 2016.
- [12] J. Hong and T. Ohtsuki, "Device-Free Passive Localization From Signal Subspace Eigenvectors," in *2014 IEEE Global Communications Conference*, pp. 430–435, Dec 2014.
- [13] Liu Heng, Wang Zheng-huan, Bu Xiang-yuan, and An Jian-ping, "Image Reconstruction Algorithms for Radio Tomographic Imaging," in *2012 IEEE International Conference on Cyber Technology in Automation, Control, and Intelligent Systems (CYBER)*, pp. 48–53, May 2012.
- [14] C. Alippi, A. Mottarella, and G. Vanini, "A RF map-based localization algorithm for indoor environments," in *2005 IEEE International Symposium on Circuits and Systems (ISCAS)*, pp. 652–655 Vol. 1, May 2005.
- [15] R. K. Martin, C. Anderson, R. W. Thomas, and A. S. King, "Modelling and Analysis of Radio Tomography," in *2011 4th IEEE International Workshop on Computational Advances in Multi-Sensor Adaptive Processing (CAMSAP)*, pp. 377–380, Dec 2011.
- [16] S. Depatla, L. Buckland, and Y. Mostofi, "X-ray Vision With Only Wifi Power Measurements Using Rytov Wave Models," *IEEE Transactions on Vehicular Technology*, vol. 64, pp. 1376–1387, April 2015.
- [17] M. Slaney and A. C. Kak, "Diffraction Tomography," in *Inverse Optics I* (A. J. Devaney, ed.), vol. 0413, pp. 2 – 19, International Society for Optics and Photonics, SPIE, 1983.
- [18] A. C. Kak and Malcolm Slaney, *Principles of Computerized Tomographic Imaging*. IEEE Press, 1972.
- [19] P. M\"uller, M. Sch\"urmann, and J. Guck, "The Theory of Diffraction Tomography," 07 2015.
- [20] K. Barkeshli and S. Khorasani, Approximate Methods, pp. 337–344. Cham: Springer International Publishing, 2015.

References



- [21] C. Alippi, M. Bocca, G. Boracchi, N. Patwari, and M. Roveri, "RTI Goes Wild: Radio Tomographic Imaging for Outdoor People Detection and Localization," *IEEE Transactions on Mobile Computing*, vol. 15, July 2014.
- [22] M. Ajmani, S. Sinanović, and T. Boutaleb, "Optimal beam radius for LED-based indoor positioning algorithm," in *2016 International Conference for Students on Applied Engineering (ICSAE)*, pp. 357–361, Oct 2016.
- [23] O. R. Popoola, W. O. Popoola, R. Ramirez-Iniguez, and S. Sinanović, "Optimization of Duty Cycles for LED based Indoor Positioning System," in *2016 International Conference for Students on Applied Engineering (ICSAE)*, pp. 368–372, Oct 2016.
- [24] E. Aguirre, J. Arpon, L. Azpilicueta, S. D. Miguel Bilbao, V. Ramos, and F. Falcone, "Evaluation of electromagnetic dosimetry of wireless systems in complex indoor scenarios with human body interaction," *Progress In Electromagnetics Research B*, vol. 43, pp. 189–209, 09 2012.
- [25] Jemai, Kumer, Varone, and Wagen, "Determination of the Permittivity of Building Materials through WLAN Measurements at 2.4 GHz," in *2005 IEEE 16th International Symposium on Personal, Indoor and Mobile Radio Communications*, vol. 1, pp. 589–593, Sep. 2005.
- [26] X. Chen, *Computational Methods for Electromagnetic Inverse Scattering*. Wiley Online Library, 2018.
- [27] S. Boyd and L. Vandenberghe, *Convex Optimization*. Cambridge university press, 2004.
- [28] "ESP32 Thing Hookup Guide." <https://learn.sparkfun.com/tutorials/esp32-thing-hookupguide>. Accessed: 2020-06-20.
- [29] "What are Near Field and Far Field Regions of an Antenna?." <https://www.everythingrf.com/community/what-are-near-field-and-far-field-regions-of-an-antenna>. Accessed: 2020-06-20.
- [30] E. Zöchmann, K. Guan, and M. Rupp, "Two-Ray Models in mmWave Communications," in *2017 IEEE 18th International Workshop on Signal Processing Advances in Wireless Communications (SPAWC)*, pp. 1–5, 2017.



Thank You

Appendix



Approximations to the Scattered Waves

Inhomogeneous Helmholtz Equation

$$(\nabla^2 + k^2)u(\mathbf{r}) = -f(\mathbf{r})u(\mathbf{r})$$

↓
wave number

Inhomogeneous Wave Equation

$$u(\mathbf{r}) = \int G(\mathbf{r} - \mathbf{r}') f(\mathbf{r}') u(\mathbf{r}') d\mathbf{r}'$$

↓ ↓
scattered field Green's function

Scattered Field

$$u(\mathbf{r}) = u_0(\mathbf{r}) + u_s(\mathbf{r})$$

↓
incident plane wave

[1] P. Müller, M. Schürmann, and J. Guck, "The Theory of Diffraction Tomography," 07 2015.



Born Approximation

- Integral of scattered field
- Magnitude of scattering is small in comparison to incident field
- Incident field is a close approximation to the total field [2]

$$u_s(\mathbf{r}) \simeq u_B(\mathbf{r}) = \int G(\mathbf{r} - \mathbf{r}') f(\mathbf{r}') u_0(\mathbf{r}') d\mathbf{r}'$$

[2] M. Slaney and A. C. Kak, "Diffraction Tomography," in Inverse Optics I (A. J. Devaney, ed.), vol. 0413, pp. 2 – 19, International Society for Optics and Photonics, SPIE, 1983.



Rytov Approximation

- Total field expressed as complex phase
- Scattered field is small compared to object scattering potential

$$u(\mathbf{r}) = \exp(\phi(\mathbf{r}))$$

↓
complex phase

$$\phi(\mathbf{r}) = \phi_0(\mathbf{r}) + \phi_s(\mathbf{r})$$

$$\phi_s(\mathbf{r}) = \frac{1}{u_0(\mathbf{r})} \int G(\mathbf{r} - \mathbf{r}') u_0(\mathbf{r}') f(\mathbf{r}') d\mathbf{r}'$$

$$\phi_s(\mathbf{r}) = \frac{u_s(\mathbf{r})}{u_0(\mathbf{r})}$$

Visible Light Communication (VLC)



- High speed data transfer ensuring a **high bandwidth**
- More accurate and efficient
- Positioning algorithms are complex – **packet loss caused by interference** when there is an overlap in the light beam regions
- MLEM (multiple LED estimation model) – simple positioning algorithm susceptible to collision
 - Simplicity compromises speed and efficiency

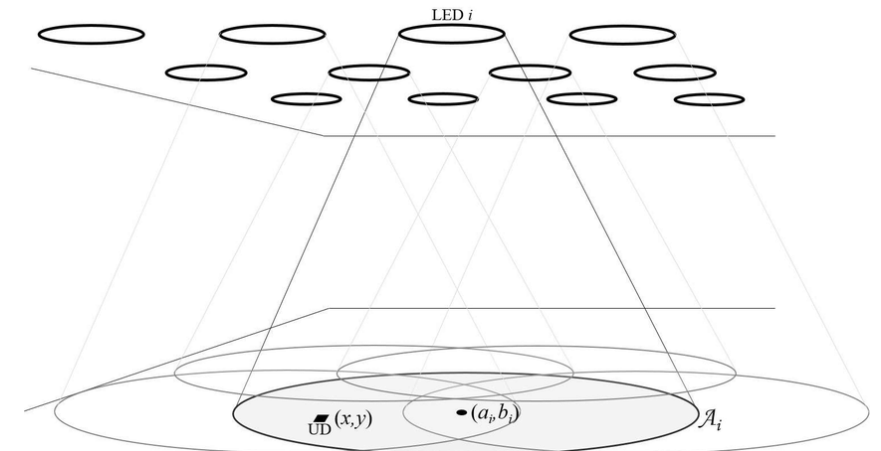


Fig. 3.2. MLEM algorithm for VLC [5]

[5] M. Ajmani, S. Sinanović, and T. Boutaleb, "Optimal beam radius for LED-based indoor positioning algorithm," in 2016 International Conference for Students on Applied Engineering (ICSAE), pp. 357–361, Oct 2016.



Hardware Details – Directional Antenna

- Gain at 2.4 GHz is 6.6 dBi
- Reactive Near Field
 - E and H fields are out of phase by 90 degrees to each other
 - To propagate, E/H fields need to be orthogonal and in phase
- Radiative Near Field Region
 - Electromagnetic fields start to transition from reactive to radiating field
- Far Field Region
 - Electromagnetic fields are dominated by radiating fields
 - E and H fields are orthogonal to each other

$$\text{Reactive Near Field Region} \leq 0.62\sqrt{\frac{D^3}{\lambda}}$$

$$0.62\sqrt{\frac{D^3}{\lambda}} \leq \text{Radiative Near Field Region} \leq \frac{2D^2}{\lambda}$$

$$\text{Far Field Region} \geq \frac{2D^2}{\lambda}$$

$$D = \text{Maximum Linear Dimension of Antenna}$$
$$f = \text{Frequency of Wi-Fi Signal} = 2.4 \text{ GHz}$$
$$\lambda = \text{Wavelength} = 0.125 \text{ m}$$

$$\text{Reactive Near Field} \leq 3.6 \text{ cm (0.036 m)}$$

$$3.6 \text{ m (0.036 m)} \leq \text{Radiating Near Field (Fresnel Region)} \leq 9 \text{ cm (0.09 m)}$$

$$\text{Far Field} \geq 9 \text{ cm (0.09 m)}$$

[13] "What are Near Field and Far Field Regions of an Antenna?." <https://www.everythingrf.com/community/what-are-near-field-and-far-field-regions-of-an-antenna>. Accessed: 2020-06-20.



Hardware Details – Directional Antenna

